Available online at www.sciencedirect.com
ScienceDirect
Phytochemistry 69 (2008) 1695–1709
PHYTOCHEMISTRY
www.elsevier.com/locate/phytochem

Identification of nickel chelators in three hyperaccumulating plants: An X-ray spectroscopic study

Emmanuelle Montargès-Pelletier [a,*], Vanessa Chardot [b], Guillaume Echevarria [b], Laurent J. Michot [a], Allan Bauer [a], Jean-Louis Morel [b]

[a] *Laboratoire Environnement et Minéralurgie, Nancy Université, CNRS, 15 Avenue du Charmois, BP 40, 54501 Vandoeuvre les Nancy Cedex, France*
[b] *Laboratoire Sols et Environnement, Nancy Université, INRA, 2 Avenue de la Forêt de Haye, BP 172, 54505 Vandœuvre les Nancy Cedex, France*

Received 31 August 2007; received in revised form 8 February 2008
Available online 26 March 2008

Abstract

We have investigated the accumulation of nickel in a hyperaccumulating plant from the Brassicacae family *Leptoplax emarginata* (Boiss.) O.E. Schulz. Two supplementary hyperaccumulating plants, which have been the subject of a high number of publications, *Alyssum murale* Waldst. & Kit and *Thlaspi caerulescens* J.&C. Presl, and a nonaccumulating species *Aurinia saxatilis* were also studied for reference. The plants were grown during 4 months in specific rhizoboxes with Ni-bearing minerals as a source of nickel. Nickel speciation was analyzed through X-ray absorption spectroscopy at Ni K-edge (X-ray absorption near edge spectroscopy and extended X-ray absorption fine structure spectroscopy) in the different parts of the plants (leaves, stems and roots) and compared with aqueous solutions containing different organo-Ni(II) complexes. Carboxylic acids (citrate, malate) appeared as the main ligands responsible of nickel transfer within those plants. Citrate was found as the predominant ligand for Ni in stems of *Leptoplax* and *Alyssum*, whereas in leaves of the three plants, malate appeared as the chelating organic acid of accumulated metal. Histidine could not be detected either in leaves, stems nor roots of any studied plant sample.

Keywords: Hyperaccumulating plants; *Thlaspi caerulescens*; *Leptoplax emarginata*; *Alyssum murale*; Chelation; Storage; Malate; Citrate; Nickel

1. Introduction

In the presence of elevated concentrations of toxic heavy metals, terrestrial plants can develop two basic strategies to protect themselves (i) exclusion or (ii) accumulation and sequestration of metals. In the exclusion strategy, the so-called nonaccumulating plants maintain metals at relatively low concentrations within their vital tissues by avoiding excessive metal uptake and transport. In the second strategy, metal-tolerant plants absorb metals through their roots and translocate them in aerial parts, stems and leaves. So called hyperaccumulating plants can thus contain up to several thousands of mg kg^{-1} of a given metal in their shoots and leaves. Hyperaccumulation of heavy metals in plants is intriguing biologically and is extremely rare (exhibited by <0.2% of angiosperms) (Baker, 1981; Baker and Brooks, 1989). About 450 taxa of hyperaccumulators have been identified today (318 are reported as Ni-accumulators). They are encountered on all continents, both in temperate and tropical environments (Baker et al., 2000). Those plants develop efficient root absorption mechanisms which allow them to specifically accumulate metals from soils even in cases where metals bioavailability is too low to affect other nonaccumulating plant species.

Ni-hyperaccumulating plants can display Ni concentrations going from several thousands of mg kg^{-1} up to 5% Ni in leaf dry matter (Baker et al., 2000; Prasad, 2005). One of the most convincing ecological explanations for hyperaccumulation of Ni and other toxic metals appears

* Corresponding author. Tel.: +33 3 83 59 62 52; fax: +33 3 83 59 62 55.
E-mail address: Emmanuelle.montarges@ensg.inpl-nancy.fr (E. Montargès-Pelletier).

0031-9422/$ - see front matter © 2008 Elsevier Ltd. All rights reserved.
doi:10.1016/j.phytochem.2008.02.009

to be related to a defensive role against herbivores or pathogens (Boyd and Martens, 1992; Pollard and Baker, 1997; Hanson et al., 2003; Prasad, 2005). A few insect species, also endemic to ultramafic environments, have evolved in parallel with these plants and have thus become specific hosts to hyperaccumulators (Mesjasz-Przybylowicz and Przybylowicz, 2001; Augustyniak et al., 2002, 2007). The existence of such closely adapted insects suggests that Ni-hyperaccumulation can benefit the plants for their defense against herbivores. In addition, hyperaccumulating plants are strongly suspected to elaborate allelopathy strategies by locally increasing Ni-phytoavailability around them, through the deposition of Ni-rich senescent leaves (Boyd and Martens, 1992, 1998; Boyd, 2004).

Understanding how plants are able to specifically accumulate or exclude essential elements and toxic metals, is fundamental for selecting species that could then be utilized for phytomanagement or phytomining (Baker and Brooks, 1989; Costa and Morel, 1993; Chaney et al., 1997; Gérard et al., 2000; Perronnet et al., 2003; Chardot et al., 2005; Echevarria et al., 2006). The conditions for their use in soil cleaning are the following: fast growing, high biomass, deep root systems and accumulation restricted to the aerial parts or harvestable parts. Many research works have been performed on these plants, not only to study their potential in polluted soils cleaning but also to determine the genomics responsible for physiological processes. Cellular and sub-cellular localization of accumulated metals has been analyzed on different accumulating species using chemical extractions of metals from separated organs of plants, or electronic or nuclear microscopies (SEM, TEM, PIXE) and coupled microanalyses. In the case of *Berkheya coddii* the highest concentrations in Ni were found in leaf margins, leaf mesophyll, and leaf epidermis (Mesjasz-Przybylowicz et al., 1994, 2001), with a maximum in the cuticle of upper epidermis (Robinson et al., 2003). In *Alyssum lesbiacum*, *A. bertolonii, A. murale, Leptoplax emarginata* and *Thlaspi gosingense*, Ni was shown to be located within the epidermal cells or in the basal compartment or pedicle of the trichomes on the leaf surface (Krämer et al., 1997; Psaras et al., 2000; Broadhurst et al., 2004). Ni pathways and storage were shown to be physically separated from Ca and Mn (Broadhurst et al., 2004). However, the precise localization of hyperaccumulated metals and their possible bonding with cell walls are still debated, as different analytical techniques involve different preparation operations that may affect the status of metals. Still, cells with higher vacuolar volume appear as preferential accumulation sites (Küpper et al., 1999, 2000, 2001) and by the comparing Ni compartmentation between nonaccumulating and hyperaccumulating species, vacuolar Ni storage in leaf cells appears as the main biochemical detoxification mechanism (Krämer et al., 2000). In view of the reactivity and limited solubility at physiological pH of most metal ions, chelation mechanisms must be operative once metals are taken up into the cell, and in particular in vacuoles. In plants, the main classes of known metal chelators are phytochelatins (peptides, oxygen and nitrogen donor ligands) and metallothioneins (sulfur donor ligands), organic acids (oxygen donor ligands), aminoacids (oxygen and nitrogen donor ligands), and other high molecular weight molecules (proteins, chaperones) implicated in the metal trafficking (Clemens, 2001).

Depending on the plant investigated, the growth conditions and the analytical technique used, various ligands have been proposed as the main chelators for Ni in hyperaccumulating plants. Histidine was identified as the main chelator of Ni in different hyperaccumulating plants of the genus *Alyssum*, and its concentration in xylem was shown to increase with Ni uptake (Krämer et al., 1996; Clemens, 2001; Ingle et al., 2005). Citric acid (Lee et al., 1977, 1978; Kersten et al., 1980) was shown as the predominant chelator for nickel transport in several hyperaccumulating plant species. In two species, *Phyllanthus serpentinus* and *Psychotria douarrei*, which are very efficient hyperaccumulators with Ni contents of 38100 and 13400 ppm, respectively, Ni–malate was evidenced as the dominating chemical form of Ni within the plant cells (Kersten et al., 1980). More recently (Mari et al., 2006; Ouerdane et al., 2006; Callahan et al., 2007), nicotianamine was presented as playing a crucial role in nickel translocation within accumulating plants. This organic ligand was evidenced through liquid chromatograpy coupled with electrospray ionization mass spectrometry.

Among analytical techniques, X-ray absorption spectroscopy (XAS) appears particularly suitable for unravelling the chemical speciation of metals in plants, as it is a nondestructive method, performed directly on the samples, without preliminary extraction or preparation This was demonstrated in various studies (Krämer et al., 1996; Persans et al., 1999; Salt et al., 1999; Sarret et al., 2001, 2002, 2003; Webb et al., 2003) which identified, histidine, citrate and malate as the most frequent ligands for Ni, Zn and Cd in the aerial parts of the plants.

In the present paper, we use the same technique to analyze the status of nickel in three different Ni-hyperaccumulators *L. emarginata*, *T. caerulescens* and *A. murale*. In comparison with other studies, we do not focus on aerial parts only, but wish to perform a complete analysis of Ni status in different parts of the plant with the aim of reaching a better understanding of Ni pathways from the soil to the plant. In that regard, in order to work with conditions that are relevant to the natural biota of hyper-accumulating plants, instead of the often used growth on hydroponic conditions, we worked in rhizoboxes, containing 4 kg of silty soil that was Ni-enriched through the presence of small nylon bags filled with Ni-bearing minerals. Rhizobox experiments were selected to obtain 5-month old plants in complete mature status, to simulate more realistic nutritional and physiological conditions. Using such a procedure, the influence of nickel availability on its speciation in various plant parts (roots, stems and leaves) can be approached.

2. Results

2.1. Ni uptake

Table 1 presents the Ni contents for the 4 different plants grown on various soils. For a given "plant–soil" system, for instance "*L. emarginata* on Ni–goethite", four rhizoboxes were prepared. As revealed by mean and standard deviation values, nickel accumulation stays in the same range of order for all rhizoboxes of a given plant–soil combination. The reproducibility between replicate experiments was assumed as good enough to allow us the use of distinct plant samples for Ni uptake measurements on one side and Ni-XAS experiments on the other side. The Ni content in the three hyperaccumulators is much higher than that in *Aurinia saxatilis* in agreement with the nontolerant nature of the latter species. The comparison between the three hyperaccumulating vegetals suggests that *T. caerulescens* is slightly less efficient in accumulating Ni than *L. emarginata*, and *A. murale*. Furthermore, whatever the plant, Ni contents are significantly higher in leaves and lower in roots. The nature of the Ni-bearing mineral introduced in the soil has a strong influence on Ni-uptake, thus revealing important variations in bioavailability. This is particularly striking in the case of Ni-bearing chrysotile, which leads to Ni-content in the plants that are equivalent to those determined after growth on the unmodified soil that contains around 20 ppm of Ni. Ni in the chrysotile structure then appears as nearly nonmobilizable. In contrast, growth on Ni–smectite leads to higher Ni uptake. The presence of easily exchangeable Ni in the interlayer space of smectite could explain such results. Finally, nickel uptake appears relatively low for all plants in comparison with other reported results on *T. caerulescens* and *A. murale* (Chardot et al., 2005; Echevarria et al., 2006). At this time, no publication concerning *L. emarginata* could be found. Other experiments on these plants (Chardot et al., 2007) show that the apparent low amounts of nickel result from a relatively short time of growth, and above all, from the growing conditions and the low bioavailability of nickel. In our case, nickel is less easily available than in the case of nickel introduction as a mineral salt.

2.2. X-ray absorption near edge structure XANES

Analysis of the XANES region of the XAS spectrum provides information on both the atomic structure and electronic properties of the nickel site. In the XANES region, the area of the pre-edge peak is related to the Ni-coordination number and geometry whereas the sharpness and amplitude of the edge depend on the chemical nature of the primary Ni ligands and on site geometry (Fig. 1). The energy position of the K-edge may also be indicative of the oxidation state of Ni (Colpas et al., 1991). In the XANES region, multiscattering processes are important and thus, this region of the X-ray absorption spectrum is sensitive to the details of the spatial arrangement and radial distances of atoms neighboring the absorbing one, and to their orientations relative to each other (Koninsberger and Prins, 1988).

XANES spectra of aqueous Ni(II)-complexes exhibit a distinct weak pre-edge feature and a strong main absorption edge feature (arrows in Fig. 1A).

The weak pre-edge peak assigned to 1s → 3d transitions is located near 8332 eV. This pre-edge feature is logically more intense for noncentrosymmetric molecules. Indeed, in the case of five-coordinate complexes with idealized trigonal-bipyramidal and square-pyramidal geometries, or four-coordinate complexes with planar geometry, XANES spectra of Ni-complexes should display a noticeable shoulder in the pre-edge region. In our case, the relatively low intensity of the pre-peak and its appearance at always the same energy 8332 eV strongly suggest that Ni remains hexa-coordinated, for all the studied samples. A similar conclusion can be reached from the XANES spectra corresponding to Ni in the various plants (Fig. 1B).

The nature of donor atoms can readily be deduced from the edge shape as demonstrated by Colpas et al. (1991).

Table 1
Ni concentrations in leaves, stems and roots, in mg kg^{-1} of fresh matter. Mean values from four rhizoboxes

Plants	Ni (mg kg^{-1})			
Soils	Raw soil	Ni–smectite	Chrysotile	Ni–Goethite
Leptoplax leaves	221.6 ± 21.3	469.3 ± 49	211.9 ± 49.8	379.7 ± 48.4
Leptoplax stems	119.1 ± 9	220.9 ± 32.1	111.5 ± 8	170.9 ± 44.6
Leptoplax roots	20.6 ± 3.8	49.4 ± 11.7	19.5 ± 2.2	32.9 ± 4
Alyssum leaves	147.5 ± 29	424.4 ± 75	165.1 ± 36.8	286.8 ± 43.8
Alyssum stems	77.4 ± 10.2	179.9 ± 29.9	72.6 ± 16.2	133.1 ± 33
Alyssum roots	18.8 ± 14.2	82.7 ± 20.5	30.2 ± 3.7	76.4 ± 38.6
Thlaspi leaves	131.1 ± 14.6	372.2 ± 91.6	155.6 ± 46.5	315.1 ± 67.1[a]
Thlaspi roots	42 ± 14.5	104.3 ± 19.9	30.3 ± 7.5	76.7 ± 27.2
Auxinia leaves	6.6 ± 1.5	15.2 ± 2.5	11.1 ± 2.1	15.9 ± 1.5
Auxinia stems	5.2 ± 1.3	10.7 ± 2.2	9.4 ± 0.5	11.7 ± 2.4
Auxinia roots	2.2 ± 0.7	8.9 ± 1.3	5.5 ± 0.3	8.9 ± 1

[a] For *Thlaspi* on Ni–goethite, only three rhizoboxes were considered.

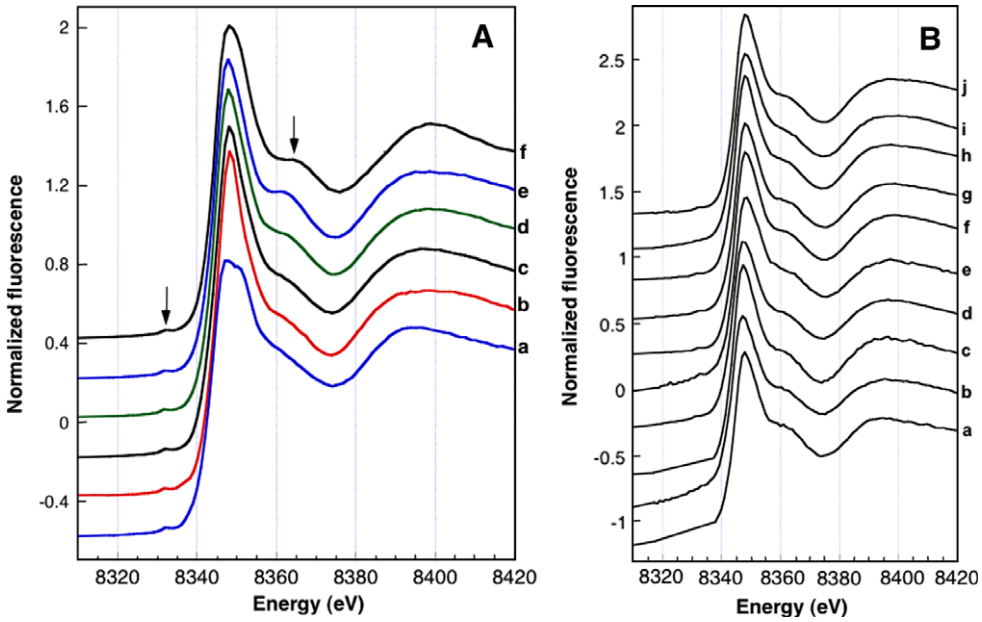

Fig. 1. (A) XANES spectra of solutions of Ni-complexes. a: Ni–histidine, b: Ni–succinate; c: Ni–glutamate; d: Ni–malate; e: Ni–citrate; f: Ni–oxalate. (B) XANES spectra of hyperaccumulating plants. a: *Alyssum m.*_leaves/chrysotile; b: *Leptoplax e.*_leaves/chrysotile; c: *Alyssum m.*_leaves/goethite; d: *Leptoplax e.*_leaves/goethite; e: *Leptoplax e.*_roots/smectite; f: *Leptoplax e.*_stems/smectite; g: *Alyssum m.*_stems/smectite; h: *Alyssum m.*_leaves/smectite; i: *Leptoplax e.*_leaves/smectite; j: *Thlaspi c.*-leaves/smectite.

Thus, for a same coordination number, the substitution of O, N ligands by S ligands provokes a 2 eV shift of the edge towards lower energies, as well as a decrease of both the maximum normalized intensity of the edge region and the edge slope. Such an evolution is not observed in the plants thus discarding the presence of S-bearing ligands.

All the spectra corresponding to carboxylic acids (Fig. 1A, spectra b–f) display similar features that are relatively close to the XANES spectrum of hydrated $Ni(H_2O)_6^{2+}$. This shows that in these complexes, Ni is octahedrally coordinated with an inner coordination geometry that is not significantly altered upon complexation with carboxylic ligands. However, on these spectra, one can notice an increase of the massive at 8362 eV with increasing complexing strength of carboxylate ligands (succinate ⩽ glutamate < malate ⩽ citrate < oxalate). This hill is related to increased multiple scattering in the signal that can be linked to the chelating power of the various ligands, malate, citrate and oxalate forming more stable multidentate complexes with cations (Strathmann and Myneni, 2004). Fig. 2 presents the organic ligands examined in solution. These ligands vary in both the number of carboxylate donor groups and the number of atoms separating the carboxylates. Some of the ligands contain an alcohol donor group adjacent to one of the carboxylates (α-OH substitution, malic and citric acids), others contain amine group (glutamic acid) or both amine and imidazole groups (histidine). In the case of Ni–glutamate complex, the amine function of glutamate molecule is supposed to be involved in the complex formation, and in that case, nickel should

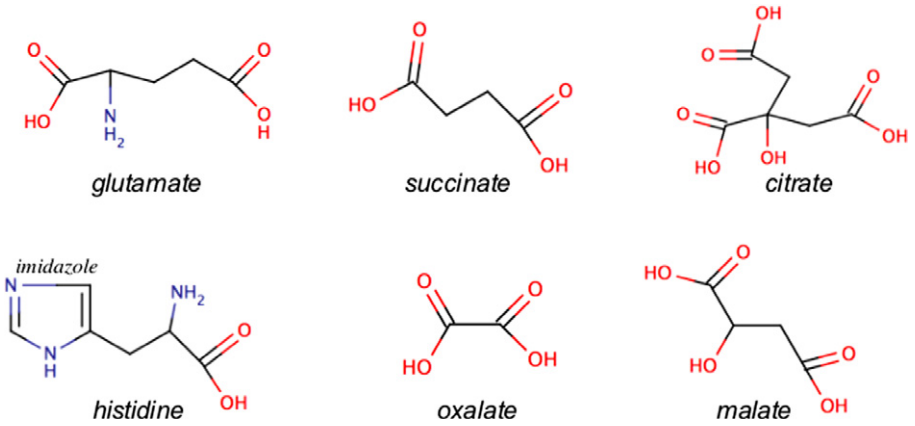

Fig. 2. Organic ligands considered for this study. Acidic forms are displayed, unmarked grey balls are carbon atoms. Only hydrogens in end of chain are presented.

be coordinated to two oxygen atoms of the carboxylate groups and one nitrogen atom of the amine group (coordination is also completed by oxygens from water molecules). XANES spectrum of Ni–glutamate complex (Fig. 1B curve c) does not display pronounced differences from the spectrum of Ni–succinate, which suggests that the presence of one nitrogen atom in the vicinity of nickel is not detectable by XANES.

In comparison with these five spectra, the spectrum corresponding to Ni–histidine (spectrum a in Fig. 1A) is markedly different. It does not display any shoulder at 8362 eV and the main peak is widened and exhibits a splitting. It must be pointed out that the Ni–histidine solution was prepared with a ratio Histidine:Ni equal to 12 and pH was adjusted at 7, in order to favour the formation of NiL_2 complex. The color change, from green to violet, reveals the formation of Ni–histidine complexes. As shown by Sakurai et al. (1978), in such complexes, Ni is octahedrally coordinated, with a slight deformation of the octahedron, to four nitrogen atoms, from the imidazole ring (see Fig. 2) and from the amine function, and to two oxygen atoms from the carboxylic function, forming a tridentate complex with histidine molecules. The shape and features of Ni–histidine spectrum are close to that already published for the $Ni(histidine)_2$ complex (Krämer et al., 2000) or for a similar complex involving imidazole group (Colpas et al., 1991), (imidazole (Im) being the ring constituent of histidine), in which nickel is coordinated to six nitrogen donor atoms.

Comparing the XANES spectra of reference compounds with those obtained on plants (Fig. 1B) shows that in all cases, i.e. within roots, stems and leaves, accumulated nickel appears predominantly complexed by a ligand of the carboxylate kind.

2.3. Extended X-ray absorption fine structure (EXAFS) of model solutions

Fig. 3A show the EXAFS oscillations extracted from the X-ray absorption spectra, plotted in k^3khi(k). Model solutions comprise weakly and strongly binding carboxylates. For succinate and glutamate, oscillations are quite symmetrical and very close to the oscillations obtained for the aqueous ions $Ni(H_2O)_6^{2+}$. In contrast, EXAFS spectra of malate, citrate and oxalate complexes, with increasing complexing strength, are characterized by a bending of the second oscillation around 6 $Å^{-1}$. The influence of complexation strength of carboxylates on the EXAFS oscillations was already observed and demonstrated (Strathmann and Myneni, 2004; McNear Jr. et al., 2007), and the EXAFS signals reported for Ni–citrate complexes are similar to those reported here.

As already observed in the XANES region, the EXAFS signal of Ni–histidine is readily distinguished from those collected for organic acid complexes. Indeed, for Ni–histidine, the second oscillation is split and the oscillations period is smaller, revealing slightly higher bonding distances between Ni and the neighboring atoms in the first coordination shell.

The radial pseudo distribution functions (RDFs) of the EXAFS spectra (Fig. 3B), obtained by Fourier transform, are one-dimension representations of the local structure around nickel cations (X-ray absorber), in the different reference solutions. These curves all show an intense peak at

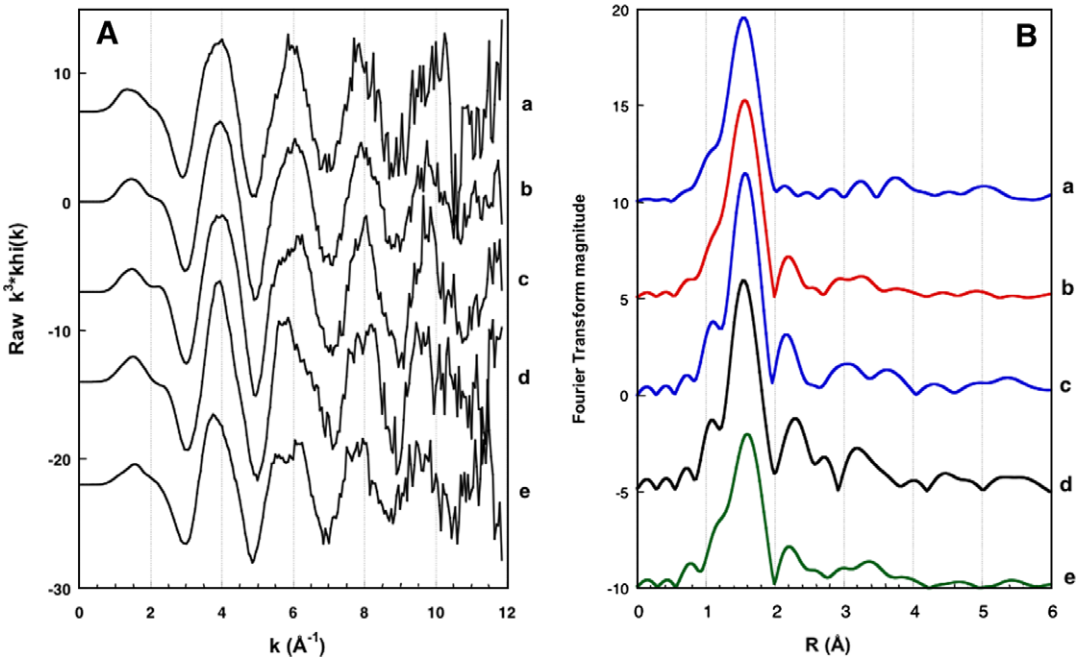

Fig. 3. (A) k^3khi(k), raw and Fourier-filtered curves; (B) Fourier transforms, magnitude and imaginary parts; a: Ni–succinate;; b: Ni–malate; c: Ni–citrate; d: Ni–oxalate; e: Ni–histidine.

1.55 Å (uncorrected of phase shift) and small peaks between 2 and 4 Å. The first peak is assigned to the contribution of the first coordination shell, i.e., oxygen atoms around Ni. The following peak at 2.2 Å is assigned to carbon atoms of the second coordination shell. Beyond the second peak, the RDFs signal is theoretically due to the sum of contributions from more distant C and O atoms as well as from multiple scattering signals, involving not only the X-ray absorber (Ni) and one single neighbour, but Ni and several neighbours (two or more), leading to scattering paths with a number of legs higher than 2.

The dissymetry in EXAFS oscillations, observed for the stronger complexants, is associated with more intense peaks on the RDFs in the 2–4 Å R range, suggesting a reinforcing of the scattering by second shell (carbon atoms) and/or further neighbouring atoms. High-distance contribution to the EXAFS signals (on k^3khi(k) as well as on RDFs curves) is unequivocally observed for a metal:ligand ratio of 1:2 for Ni–citrate complexes (Strathmann and Myneni, 2004) revealing the structure of such organometallic complexes.

A qualitative analysis of EXAFS oscillations, employing a Fourier filter (Fig. 4), shows the relative contributions of the first and next coordination shells. Fourier backfiltering was carried out on different R ranges, with increasing width, and the resulting filtered curves are displayed on Fig. 3B. The first filtered k^3khi(k) curve (1), corresponding to the R range 0.8–2 Å, is very close to the raw EXAFS signal, in terms of amplitude (Fig. 4A and Fig. 4B curve 1), which shows that the raw EXAFS signal mainly results from the scattering of ejected photoelectron by the first shell of neighbouring atoms (oxygens in that case).

Extending the back-filtering range (curves 2–4 in Fig. 4B) reveals that the dissymetry observed for Ni–citrate is due to scattering paths with distances higher than 3 Å, i.e. beyond the second coordination shell. The third graph

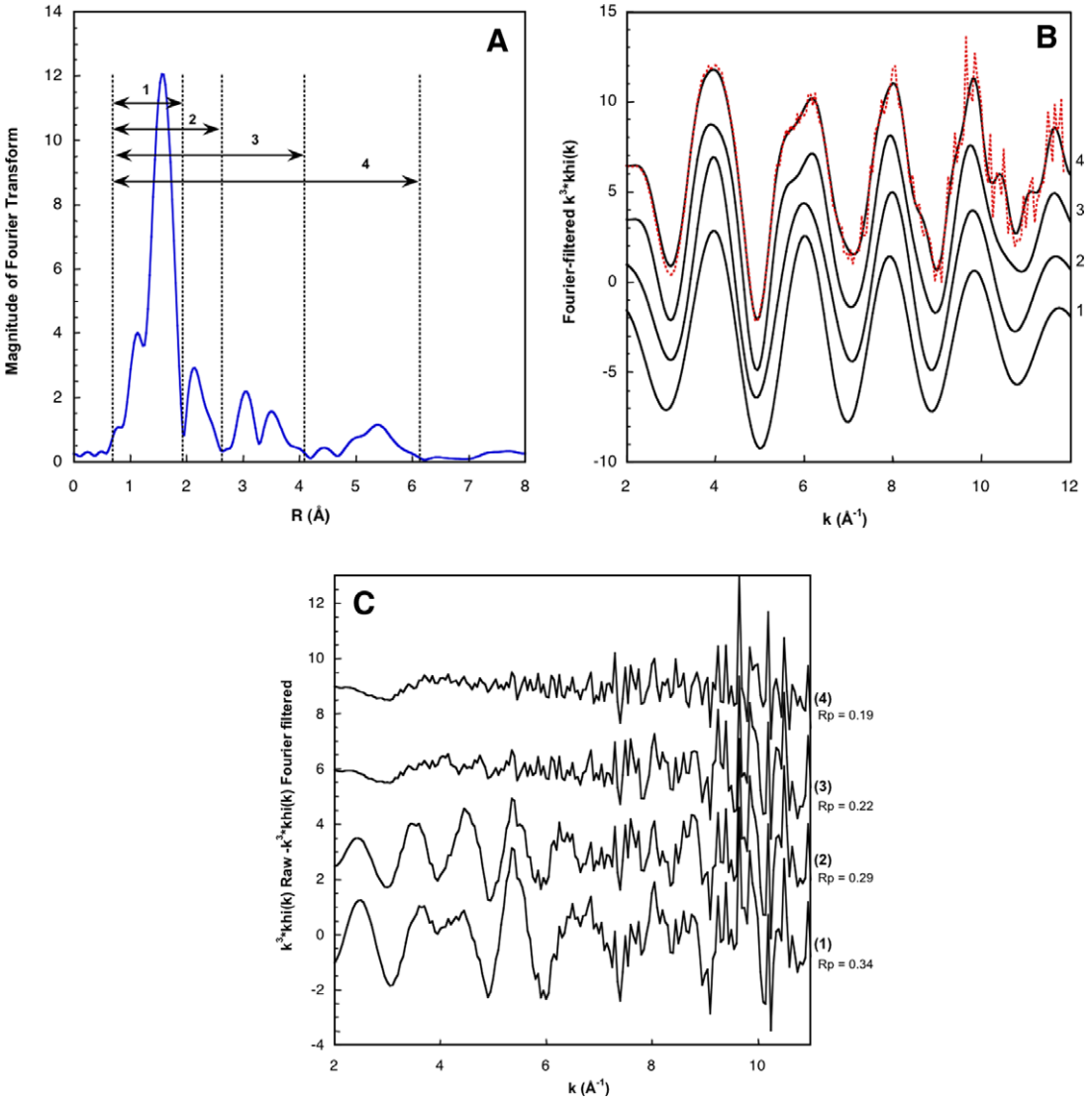

Fig. 4. (A) Fourier transform of Ni–citrate solution. (B) Fourier Filtered EXAFS oscillations for different ranges of filtering 0.7–1.9; 0.7–2.6; 0.7–4.1 and 0.7–6.1 Å. The last filter is compared with raw EXAFS oscillations. (C) difference curves (Raw k^3khi - filtered k^3khi).

(Fig. 4C) presents the calculated difference curves from the subtraction of Fourier filtered curves to raw signal and this, for the four distinct *R* ranges. The difference curve obtained from the subtraction of filter 2 (0.8–3 Å) displays noticeable oscillations at low *k*, demonstrating the presence of true EXAFS signal, assigned to neighbouring atoms beyond the second coordination shell. As soon as the third peak is taken into account (filter referred to as 3, Fourier backfiltering on 0.8–4.1 Å *R* range), the difference curve is mainly constituted by noise at high *k* values.

The small peaks of the Fourier transform at higher R values (from 4 to 6 Å) may arise from distant C and O atoms as well as from multiple scattering paths. This high distance signal can be explained by the formation of a more rigid structure in the case of multidentate complexes of nickel with malate, citrate and oxalate. The higher degree of rigidity of complexes can be due to inner rigidity of the molecule (oxalate) or to the presence of an alcohol group in the vicinity of the complexing carboxylic function (citrate and malate). However, difference curve (4) only displays noisy signal at high k values, incompatible with oscillations due to scattering by light atoms such as oxygen and carbon.

On the basis of this qualitative analysis, it appears that Fourier backfiltering should be performed on the *R* range [0.8–4] Å. Structural information can then be deduced from the analysis of such Fourier filtered k^3khi(*k*) curves, on the basis of theoretical fitting. For that purpose, crystallographic models for Ni–malate and Ni–citrate complexes (Ni:L = 1 for both complexes) (Baker et al., 1983; Zhou et al., 2002) were used to build theoretical EXAFS oscillations at Ni K-edge. FEFF calculations, on the basis of FEFF6 module included in ARTEMIS software, revealed similar theoretical EXAFS signals for both complexes. Actually, FEFF6 calculates theoretical scattering signal from a list of scattering paths (single and multiple, path number = 2 or >2), deduced from crystallographical data and atomic positions. Both crystallographical models from Ni–citrate and Ni–malate crystals give similar, or almost identical list of scattering paths in terms of distance, nature, and contribution to the EXAFS signal. According to the crystallographic data reported for Ni–organic acids complexes, in both cases Ni is first surrounded by two neighbours shells, composed of six oxygen atoms (2.02–2.08 Å for Ni–malate; 2.01–2.08 Å for Ni–citrate) and four carbon atoms (2.80–3.01 Å for Ni–malate; 2.80–3.03 for Ni–citrate) respectively. These single scattering paths are followed by an almost continuous series of multiple and single scattering paths. The presence of a supplementary carboxylic group for citrate molecule may induce supplementary scattering paths or more consequent scattering paths in terms of contribution to the EXAFS oscillations. However, the comparison of paths lists created by FEFF on the basis of crystallographical data did not reveal noticeable differences between Ni–malate and Ni–citrate in terms of neighbours distribution. Furthermore, none of these models was able to reproduce the dissymetry in EXAFS oscillations around 6 $Å^{-1}$.

The crystallographic model of Ni–malate was still conserved as the starting point for the theoretical fitting of Ni–malate and Ni–citrate experimental data. To reproduce the difference between Ni–malate and Ni–citrate spectra in terms of numbers of neighbours and neighbours distances, we performed signal fitting taking into account relatively long distances, above the second coordination shell. In such conditions, fitting was rather difficult due to the high number of scattering paths in the selected fitting range, i.e. [1–4] *R* range. Fitting was then carried out by reducing as much as possible the number of different scattering paths and restricting the scattering signal to single scattering paths. Also, as the main objective of this fitting procedure was to unravel structural differences between Ni–malate and Ni–citrate complexes, the scattering paths selected were identical for both samples. Fitting results are presented on Fig. 5 (plots A and B for Ni–malate; plots C and D for Ni–citrate), whereas Table 2 summarizes the fitting parameters for both Ni-complexes. Although such fitting results do not actually solve the structural models for Ni–malate and Ni–citrate, they confirm the fact that neighbours beyond the second shell, constituted by carbon atoms, can not be neglected in the fitting exercise. According to the analysis presented here, the differences between Ni–citrate and Ni–malate would be due to differences in numbers, and distances in the second and third shells. Ni–citrate apparently displays higher numbers of neighbours which may explain a stronger bending of EXAFS oscillations around 6 $Å^{-1}$.

2.4. EXAFS oscillations of plant samples

2.4.1. Plants grown on Ni–smectite

As plants grown on Ni–smectite display the highest Ni uptakes (Table 1), EXAFS spectra were preferentially collected on these plant samples. Fig. 6 displays the data obtained for the three plants grown on Ni–smectite, for different organs, stems, leaves or roots. Data for roots samples were collected for *L. emarginata* only. However, due to the low Ni content within roots, the collected spectra displayed a very low signal:noise ratio, and despite longer accumulation times, and a high number of scans, the signal quality could not be highly improved (curve f).

All the curves plotted in Fig. 6A display a dissymetry of the second EXAFS oscillation, indicating that chemical speciation of nickel in those different plant samples implies the complexation with a more complex molecule than water, such as an organic ligand, with characteristics close to citrate or malate. The radial structure functions of the EXAFS spectra, obtained through Fourier transform, display a major peak centered at 1.55 Å. The individual fitting of this major peak, which is also the major scattering contribution, reveals the presence of 6 oxygen atoms with Ni–O distances ranging from 2.03 to 2.06 Å (Table 3) which is consistent with the model of NiO_6 octahedron (Martell and Hancock, 1996).

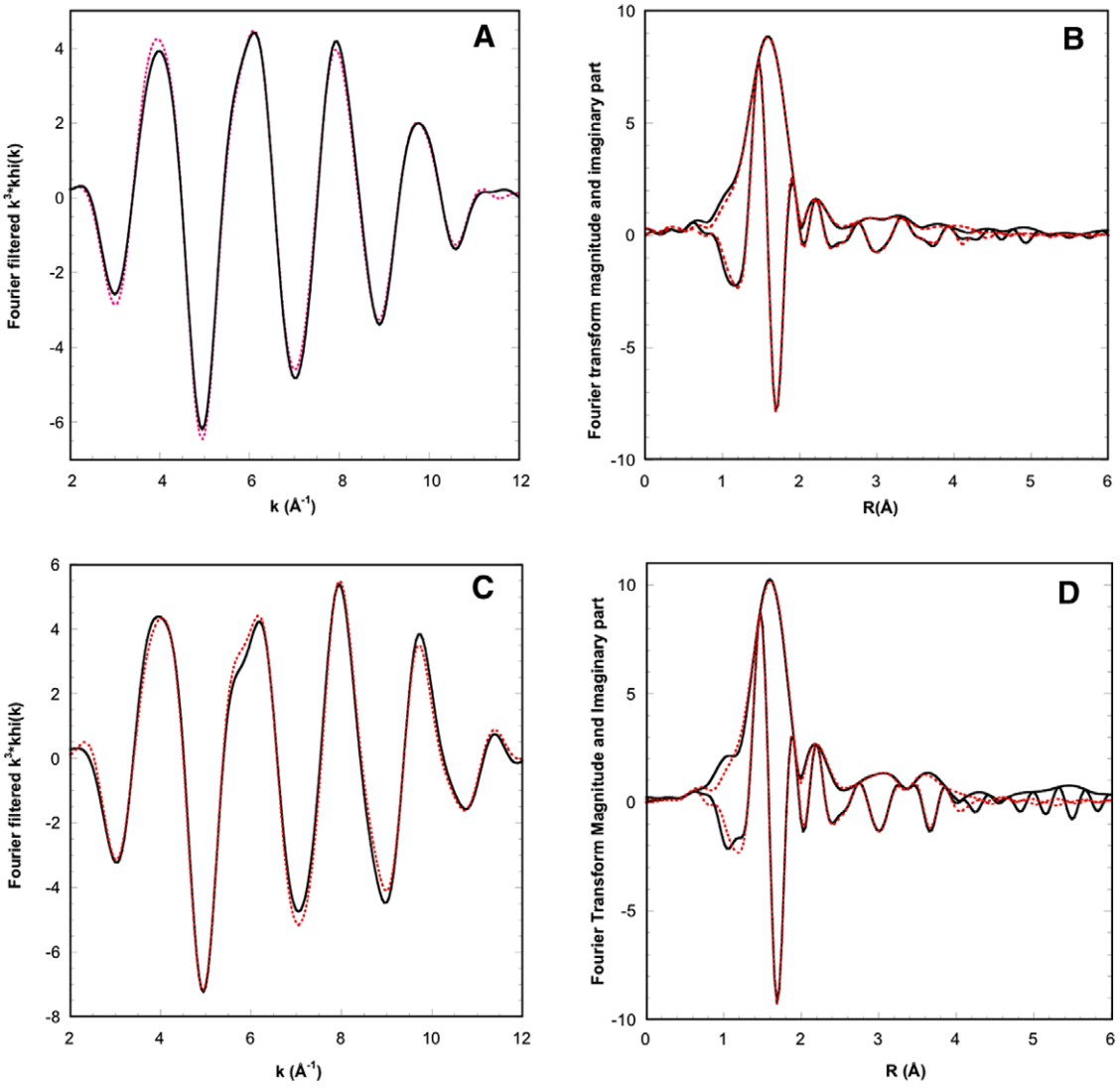

Fig. 5. Theoretical fitting of Ni–malate and Ni–citrate experimental signals: (A) Fourier filtered, (B) Fourier Transform, (C) Fourier filtered k^3khi(k) and (D) Fourier Transform, for Ni–malate. The Fourier Transform display both real and imaginary parts.

Table 2
Fitting parameters for Ni–malate and Ni–citrate

	N_i	R_i (Å)	σ_i^2 (Å^2)	Number of legs
Ni–malate				
Oxygen	6	2.04	0.006	2
Carbon	2	2.82	0.078	2
Carbon	1.2	3.37	0.002	2
Oxygen	1.5	3.61	0.003	2
Oxygen	3	3.81	0.003	2
Oxygen	3	4.39	0.004	2
Ni–citrate				
Oxygen	6	2.04	0.004	2
Carbon	4	2.77	0.006	2
Carbon	2	3.30	0.002	2
Oxygen	2	3.68	0.002	2
Oxygen	6	4.23	0.003	2
Oxygen	5	4.37	0.002	2

N_i: number of neighbours for the ith shell surrounding Ni central atom; R_i: mean distance between N_i and backscattering atom of the ith shell;. σ_i^2: Debye–Waller factor (Å^{-2}) of the ith shell.

Theoretical fitting of further coordination shells was rather difficult for plant samples due to the rather low signal to noise ratio. Using a qualitative analysis step, identical to that developed for reference solutions (Fig. 4) it was evidenced that scattering neighbours beyond the second shell of atoms must be considered for a proper exploitation of the curves. Fourier filtering was then run on the same R range 1–4 Å as for reference solutions.

EXAFS oscillations obtained for plant samples were then compared to those obtained for reference solutions, after Fourier filtering to remove high frequency noise. Fig. 7 presents the superimposition of the XAS signal for *Thlaspi* leaves with that of Ni–malate solution. For filtered k^3khi(k) curve as for Fourier transform magnitude and imaginary part, there is a good adequation of the selected reference with the leaves of *Thlaspi*. In the leaves of *Thlaspi*, nickel appears mainly associated with malate ligands.

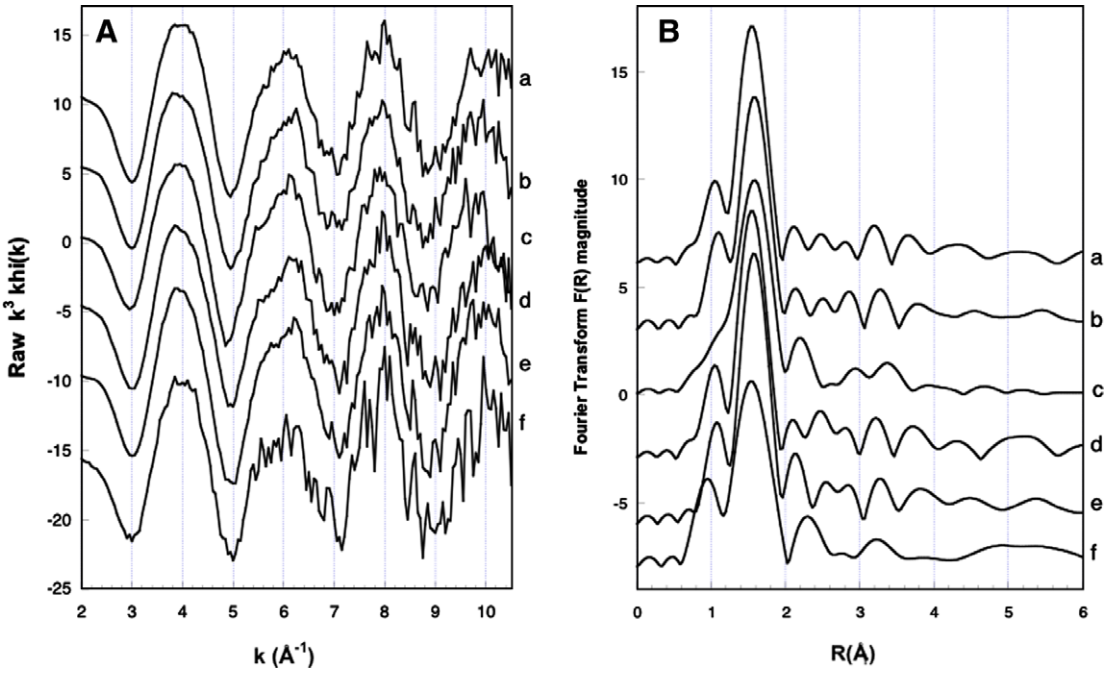

Fig. 6. (A) k^3khi(k), raw curves; (B)-Fourier transforms, magnitude; a: *Thlaspi c.* leaves Ni–smectite; b: *Alyssum m.* leaves Ni–smectite; c: *Leptoplax e.* leaves Ni–smectite; d: *Alyssum m.* stems Ni–smectite; e: *Leptoplax e.* stems Ni–smectite; f: *Leptoplax e.* roots Ni–smectite.

Table 3
Fitting parameters for the first shell of neighbours around Ni within plants

Samples	N	σ^2 (Å^2)	R (Å)
Ni–smectite			
Leptoplax leaves	6	0.003	2.052
Leptoplax stems	6	0.003	2.029
Leptoplax roots	6	0.002	2.051
Alyssum leaves	6	0.002	2.064
Alyssum stems	6	0.002	2.053
Thlaspi leaves	6	0.004	2.047
Chrysotile			
Leptoplax leaves	6	0.002	2.067
Alyssum leaves	6	0.002	2.064
Ni–goethite			
Leptoplax leaves	6	0.003	2.049
Alyssum leaves	6	0.004	2.005

N: number of neighbours. σ^2: Debye–Waller factor(Å^{-2}). R (Å) Ni–O distance.

For *Leptoplax* and *Alyssum* leaves, malate also appears as the main complexing ligand (Fig. 8A, data for *Alyssum* leaves not shown) whereas Ni–citrate appears as the main chemical form of nickel within stems of *Leptoplax* and *Alyssum* (Fig. 8B). For plants grown on Ni–smectite, citrate then appears as the main chelator for nickel within stems, whereas malate predominates nickel complexation within leaves.

2.4.2. *Leptoplax grown on Ni–goethite and chrysotile*

Raw EXAFS signals obtained for *Leptoplax* leaves from plants grown on different media, with a different source of nickel (Fig. 9A). Leaves from *Leptoplax* grown on chrysotile, display a very low signal:noise ratio, in relation with the lower amount of nickel stored within the aerial parts (Table 1). The analysis of the first shell yields similar results as those obtained previously for plants grown on Ni–smectite, i.e. Ni is octahedrally coordinated with six oxygen atoms, with bonding distances ranging between 2.03 and 2.06 Å (Table 3). The comparison of Fourier filtered signal obtained from *Leptoplax* leaves grown on Ni–goethite with this Ni–citrate in solution, demonstrates the likely similarity of nickel speciation within these two samples, suggesting that citrate can also be encountered as the major ligand of nickel within leaves of *Leptoplax* (Fig. 9B).

3. Discussion

The analysis of XANES spectra as well as analysis of first coordination shell demonstrated unambiguously that nickel is predominantly six-coordinated with oxygen atoms, from both water molecules and carboxylic ligands. The distinction between carboxylic ligands can be made if considering further shells of neighbouring atoms, i.e., carbon and oxygen atoms from further shells than the first two shells of coordination.

On the basis of curves superimposition, citrate and malate appear as the main chelators of nickel within stems and leaves of the studied hyperaccumulating species. Histidine was rapidly ignored as a model for Ni complexation, as none of the EXAFS data obtained for plants samples could be compared to Ni–histidine EXAFS curve (Figs. 6–9 for plant samples; Fig. 3, curve e for histidine). This is in contradiction with previous findings where histidine

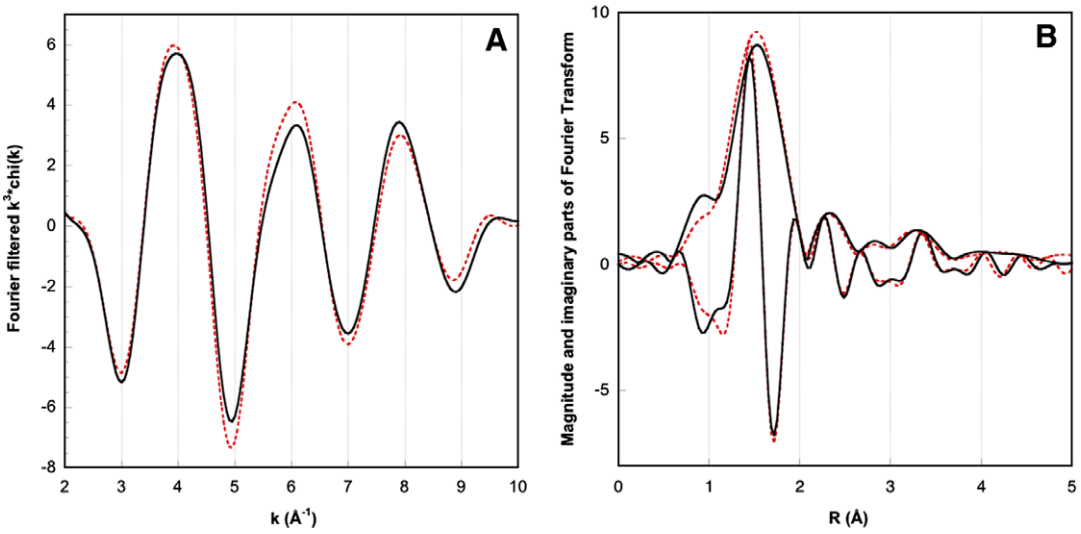

Fig. 7. Comparison of filtered k^3khi(k) oscillations (A) and Fourier transforms (B) from Ni in *T.c.* leaves (full line) and Ni–malate (dotted line) complex in aqueous solution.

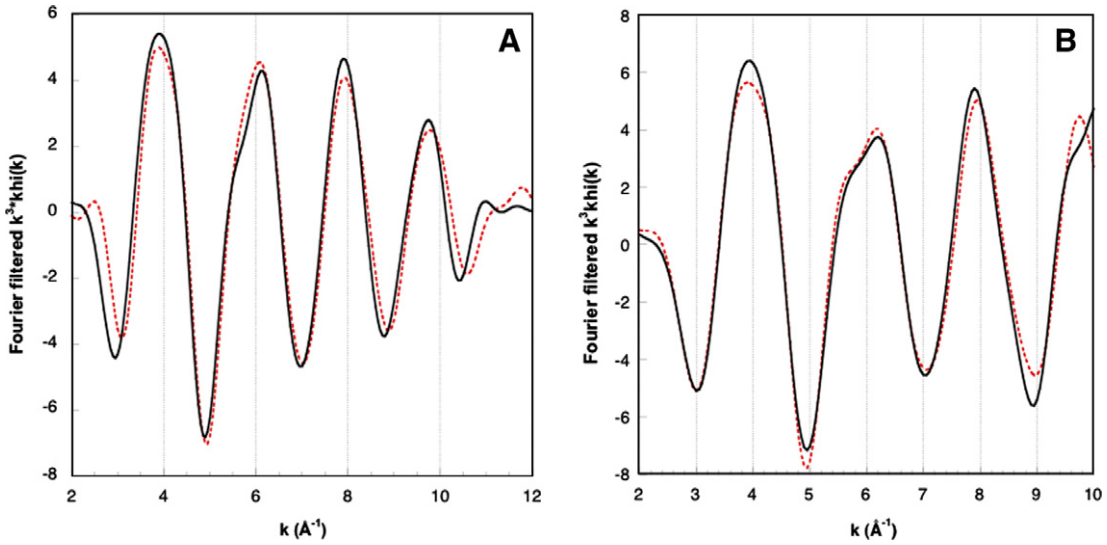

Fig. 8. Comparison of filtered k^3khi(k) oscillations from Ni complex in aqueous solution (dotted line) and Ni complex within *Leptoplax emarginata* (full line). (A) Ni in *Leptoplax emarginata* leaves and Ni–malate solution; (B) Ni in *Leptoplax emarginata* stems and Ni–citrate solution.

was proposed as the main Ni chelator in leaves of *Alyssum* species (*A. murale, A. lesbiacum, A. montanum,* and *A. bertolonii*) (Krämer et al., 1996). This conclusion was primarily deduced from a strong correlation between Ni-uptake and histidine amount in the plant and confirmed by XAS measurements. In that latter part, the authors claimed that it was possible to fit their experimental EXAFS oscillations with a structure consistent with Ni–histidine complex. However, no EXAFS spectrum of aqueous Ni–histidine was provided whereas the published spectrum is markedly different from EXAFS signal collected for Ni–histidine in solution (Fig. 3, spectrum e). Furthermore, distinguishing O from N neighbours in an EXAFS analysis appears rather difficult, considering the very similar backscattering amplitude and phase of these two atoms. For these reasons, we would tend to believe that the speciation of Ni as Ni–histidine in plants can be seriously debated.

In parallel to these experiments in rhizoboxes, hydroponically grown plants were tested. These experiments included the measurement of organic acids in hyperaccumulating species after 1 week (data not shown). This parallel experiment demonstrated that the correlation between organic acids levels within plants and nickel amounts was useless in our case as the relatively low uptake of nickel would result in ligand:metal ratios superiors to 100:1.

The fact that citrate is the predominant complexing molecule for nickel within stems can be reinforced by the study of *Sebertia accuminata*, a hyperaccumulating tree. Indeed, the analysis of the latex demonstrated that citrate was the

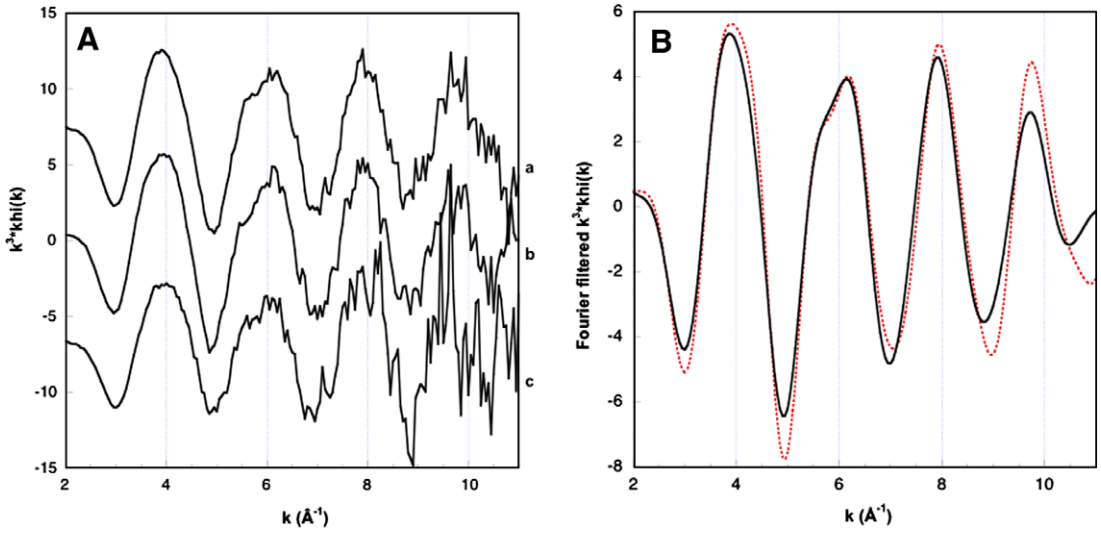

Fig. 9. (A) Filtered k^3khi(k) oscillations from Ni in *Leptoplax* leaves; a: Grown on Ni–goethite, b: grown on Ni–smectite, c: grown on chrysotile. (B) Comparison of Ni–citrate in solution with leaves from *Leptoplax* grown on Ni–goethite.

main nickel chelator (Schaumlöffel et al., 2003). A tentative link could be drawn between these results and ours. One of the possible explanations for the presence of citrate in the transporting organs could be related to the fact that it forms more stable complexes with nickel cations than malate, which facilitates transport. In vacuolar compartments, a change of speciation is observed and nickel appears mainly complexed with malate. This molecule is known to play a major role in stomata function. Guard cells display a higher vacuole:cytoplasm volume ratio, with relatively high concentrations in malate and for this reason they appeared at first sight as good candidates for nickel storage. Indeed, an opposite reasoning was proposed by Psaras et al. (2000). As they evidenced the exclusion of nickel from guard cells in eight accumulating plant species, they concluded that the crucial function of stomata and associated guard cells was not compatible with nickel accumulation. One first hypothesis would be the consumption of malate ligands by nickel cations that may interfere with the role of this organic acid in the regulation of transpiration. Their works as well as those of Broadhurst et al. (2004) demonstrated that trichomes were not systematically involved in the storage of nickel, and because of their early evolution towards inert organs, they do not display the necessary properties for mechanical and physiological accumulation of nickel.

Citric and malic acids are not specific ligands, Ni is defined as a metal that exhibits weaker binding affinities, so what guides this metal towards storage cell? As it was previously noticed by Ueno et al. (2005), the detoxication mechanism does not consist only in the complexation of nickel in order to reduce its activity. Indeed, complexation of nickel by organic ligands is a consequence of their joint presence in vacuolar compartments of the cell. The way nickel is transported to the vacuoles is still not elucidated. Ni contents were too low in roots for a correct signal collection, however XANES spectrum for roots of *L. emarginata* is similar to other spectra acquired for stems or leaves, strongly suggesting a complexation with ligands of carboxylate kind.

X-ray absorption spectroscopy display the main advantage to detect the predominant species, and low contents in metal can be detected and studied in terms of chemical speciation. This technique is an in situ method and minimizes the modifications of the biological material. The first advantage can also be assumed as a limitation for the identification of minor chemical forms of accumulated metals, ligand identification is highly dependent of the solutions employed for references. For these two limitations, XAS experiments might be completed by indirect methods based on hydrophilic interaction liquid chromatography (Schaumlöffel et al., 2003; Vacchina et al., 2003; Ouerdane et al., 2006). Indeed the reported technique Q-TOFMS/MS after isolation by 2D size exclusion-hydrophilic interaction can provide the identification of the different chemical species. However those methods highly suffer from the relatively low percentage of nickel recovery. Thus, the identification of [Ni(nicotianamine)$_2$] complex by ESI-MS (electrospray ionisation mass spectrometry) was performed on 0.3% of recovered Ni. The properties of the column used for separation, such as the separation range may exclude small complexes such as Ni(citrate). In his review Collins (2004) demonstrate that chromatographic techniques have to be handled with high precaution as separation results may be highly selective and resulting extracts are not always representative of the different chemical species present in the vacuoles. For us, separation techniques provide complementary tools for the knowledge of metals speciation as they might detect supplementary species. However, they can not be as quantitative as they pretend due to the imperfection of the separation method.

4. Conclusions

From the study of nickel speciation within hyperaccumulating plants through X-ray absorption spectroscopy, we demonstrated that nickel was stored as nickel-malate complexes within leaves of three different hyperaccumulating plants, *A. murale, L. emarginata* and *T. caerulescens*. In contrast, citrate appears as the main complexing ligand within stems of *Alyssum* and *Leptoplax*. The combination of precise XANES experiments with careful EXAFS data fitting appears as a fruitful tool for such studies. However, though we have determined the nature of the complexing ion, no definite answer could be provided regarding the variation of the metal: ligand ratio. Such information that might be obtained by working systematically with model solutions of varying metal/ligand ration could be of importance as this ratio strongly influences the chemical activity of the metallic cation in the vacuolar solution and therefore plays a role in detoxication mechanisms. Furthermore, in order to unravel the complete nickel pathway, it would certainly be relevant to supplement the bulk EXAFS data presented here with micro-XAS experiments using microbeams of a few square microns to study in detail the evolution of nickel speciation with its localization in the plants. Due to the higher probability of beam damage in the case of focused-beam experiments, XAS spectra collection in the dispersive mode would be preferred as it could prevent any modification of the biological object. As far as the extraction of nickel from the soil is concerned, it would also be interesting to study in detail the modification of the Ni-bearing minerals after plant growth.

5. Experimental

5.1. Plants, rhizoboxes

Different hyperaccumulating plants were selected, all from the Brassicaeae family: *L. emarginata* (Boiss.) O.E. Schulz, *Alyssum murale* Waldst. & Kit. and *T. caerulescens* J.&C. Presl. The phytoextraction potential of these three species was compared in a previous work (Chardot et al., 2005). A nonaccumulating species (*A. saxatilis*, Brassicaceae) was selected as reference. Seeds of *L. emarginata* were collected in late July 2002 from the Katara Pass area of the Pindus Mountains near Metsovo in northern Greece, at an altitude of 1670 m, on serpentine soils with low nutrients (especially Ca) and low summer water contents. Seeds of *T. caerulescens* were collected on the serpentine site of Bergenbach (Ordern, Vosges Mountains France), and seeds of *A. murale* were collected on the serpentine soils of Pogradec (Albania) (Shallari et al., 1998; Chardot et al., 2005, 2007; Bani et al., 2007). Seeds were stored at +4 °C before use in order to favor their further germination. Seeds of the four plant species were germinated on an organic material (potting compost with low total Ni content of 4.6 mg kg^{-1}) for about 20 days, and then two seedlings were transplanted into the rhizoboxes.

Rhizoboxes contained 4 kg of silty soil. The soil samples were collected in Augny (Moselle, France) from the Ap horizon (0–20 cm) of an acidic quartz silt soil (Haplic Luvisol, WRB, FAO). This soil was characterized by a low Ni content (21.4 mg kg^{-1}) and a very poor Ni retention ability. The soil samples were air dried, and sieved to 5 mm before use.

Nylon bags containing Ni-bearing minerals were placed in the soil at 10 cm below the surface. We selected three Ni-bearing minerals reflecting different ultramafic pedological contexts and also showing increasing degree of availability: i) a synthetic nickeliferrous goethite (oxi-hydroxide) with 1.6% of Ni; ii) natural chrysotile (fibrous serpentine, phyllosilicate) with 0.4% of Ni; iii) natural nickeliferrous smectite with 2.3% of Ni. Nickel status in these three minerals was studied through Transmission Electron Microscopy – Energy Dispersion X-ray Spectroscopy, X-ray Photoelectron Spectroscopy, and Cation Exchange Capacity measurements (results not shown). The smectite mineral phase displays the highest content of easily available nickel as Ni^{2+} cations take part in the exchangeable cation capacity of the smectite (12 mmol/100 g exchangeable Ni corresponding to about 2.7% of the whole Cationic Exchange Capacity). No exchangeable nickel could be detected from chrysotile and Ni–goethite. Nickel in goethite and chrysotile minerals was shown to be inserted in the crystallographical structure of iron-oxi-hydroxide and phyllosilicate (octahedral sheet), replacing iron and magnesium respectively.

The culture was conducted for 5 months (from April to September 2005) in a greenhouse with temperature control (minimal temperature 20 °C). No supplemental light was provided. The soil moisture was maintained up to 60% of the soil water holding capacity with deionised water. Soils were fertilized twice during the experiment (2 and 4 months after transplantation) with nitrogen as NH_4NO_3 (30 mg kg^{-1}), phosphorus (20 mg kg^{-1}) and potassium (30 mg kg^{-1}) as KH_2PO_4, and sulfur as $MgSO_4$ (30 mg kg^{-1}) in order to obtain optimal growth conditions for plants.

One third of the rhizoboxes was dedicated to XAS experiments, the rest was used for the quantitative determination of nickel accumulation within plants.

5.2. Mineralization, nickel dosage

After 5 months of culture, plant roots, stems and leaves were collected, separated, carefully washed with deionised water, oven-dried at 70 °C for 48 h, and crushed. Then, 0.5 g-samples of plant dry matter were acid-digested at 250 °C in 2 ml of concentrated H_2SO_4 (98%), 6 ml of concentrated HNO_3 (98%) and 6 ml of H_2O_2 (30%). The final solutions were filtered and completed up to 25 ml with deionized water. Ni concentration in solution was measured with an Atomic Emission Spectrometer (ICP-AES, Liberty II, Varian).

5.3. X-ray spectroscopy

5.3.1. Model solutions

Several solutions of Ni-complexes were prepared as model compounds for X-ray experiments. These solutions were prepared at pH 7.0 with metal/ligand ratio equal to 1/10 to enhance multidentate complex formation in solution. Six different ligands were selected: malate, citrate, glutamate, succinate, oxalate and histidine. These ligands were selected on the basis of their occurrence in roots (Jones, 1998).

5.3.2. Preparation of plant samples

In the minutes following harvesting, plants were gently rinsed with distilled water and the different parts: roots, stems and leaves were separated. Roots, Stems and Leaves were then ground and compacted into a teflon sample holder covered with a thin layer of Kapton (7.5 μm). These two operations were performed in liquid nitrogen, with care to keep the samples frozen all the time. Samples were kept at 77 K prior to measurement in a dedicated Dewar. For X-ray absorption experiments, samples were cooled at the same temperature using a liquid nitrogen cryostat.

5.3.3. XAS experiments

Data collection was performed ar beamline 16.5 at CLRC Daresbury Synchrotron Radiation Source, UK, (2 GeV, 150 mA). This beamline, dedicated to ultra-dilute spectroscopy was particularly adapted for the study of nickel local environment in plants. The detection limit for the collection of XAS spectra at Ni K-edge was appreciated to be 50–100 ppm (private communication from the beamline scientist Robert Bilsborrow). The X-rays were monochromatized using a Si(220) double crystal. Three to seven scans were collected and averaged per sample. Samples were kept at 45 angular degrees to the incident beam to collect spectra in fluorescence mode using a 30-element Ge solid-state detector with high count-rate electronics, (200 kHz per channel). Collecting time was set to 10 s.

XANES and EXAFS data were reduced using standard procedures normalization performed with Bruce Ravel and Matthew Newville programs ATHENA and ARTEMIS (Newville, 2001; Ravel and Newville, 2005). Spectra were background subtracted, and normalized. A spline function was fit through the absorption envelope and subtracted from each spectrum. To transform data from energy space E (eV) to wavevector space k (Å^{-1}), E0 edge energy was chosen in the higher part of the edge step, at 8343 eV. The resulting khi(k) function was weighted by k^3 to avoid oscillations damping at high k values (other parameters: no low clamp: none; strong high clamp; Fourier transform on the range [1–11.3] Å^{-1}, Kaiser Bessel shape parameter = 1; Back fourier filtering $\Delta R = 0.1$, R range [0.8–4] Å).

Theoretical spectra could be calculated following the crystallographical reduced data from Ni–citrate and Ni–malate complexes (Baker et al., 1983; Zhou et al., 2002) and using ARTEMIS (includes ATOMS, FEFF6 packages). Individual scattering paths were selected for fitting on the basis of the number of implied scattering legs (simple scattering, $n = 2$; multiple scattering, $n > 2$), of their relevance and relative contribution in EXAFS signal (calculated by FEFF).

Acknowledgements

This work was financially supported by CNRS-INSU, through the national research programm ECCO ''Ecosphere continentale: processus et modélisation''. The European Union, via Integrated Activity on Synchrotron and Free Electron Laser Science (IA-SFS) under the EC Framework Programme 6 (FP6), funded our experiments in SRS, Daresbury UK, covering travel and lodging expenses. The authors acknowledge the Daresbury Synchrotron Radiation Source for the provision of beamtime. We gratefully thank Shusaku Hayama and Robert Bilsborrow for their technical support on beamline 16.5 at SRS. Samples preparation benefited from the enthusiastic help of Marie-Claude Rouillier, Elisabeth Schouller, Isabelle Bihannic, and Manuel Pelletier. We also thank David S. Salt for advices on sample preparation.

References

Augustyniak, M., Mesjasz-Przybylowicz, J., Nakahashi, Y., Dybowska, M., Przybylowicz, W.J., Migula, P., 2002. Food relations between *Chrysolina pardalina* and *Berkheya coddii*, a nickel hyperaccumulator from South African ultramafic outcrops. Fresenius Environ. Bull. 11, 85–90.

Augustyniak, M., Migula, P., Mesjasz-Przybylowicz, J., Tarnawska, M., Nakonieczny, M., Babczynska, A., Przybylowicz, W.J., Augustyniak, M.G., 2007. Short-term effects of dimethoate on metabolic responses in *Chrysolina pardalina* (Chrysomelidae) feeding on *Berkheya coddii* (Asteraceae), a hyper-accumulator of nickel. Environ. Pollut. 150, 218–224.

Baker, A.J.M., 1981. Accumulators and excluders – strategies in the response of plants to heavy metals. J. Plant Nutr. 3, 643–654.

Baker, A.J.M., Brooks, R.R., 1989. Terrestrial higher plants which hyperaccumulate metallic elements – a review of their distribution, ecology and phytochemistry. Biorecovery 1, 81–126.

Baker, A.J.M., McGrath, S.P., Reeves, R.G., 2000. Metal hyperaccumulator plants: a review of the ecology and physiology of a biological resource for phytoremediation of metal-polluted soils. In: Norman, T., Gary, B. (Eds.), Phytoremediation of Contaminated Soil and Water. CRC Press, Boca Raton, FL, USA, pp. 85–107.

Baker, E.N., Baker, H.M., Anderson, B.F., Reeves, R.G., 1983. Chelation of nickel(II) by citrate. The crystal structure of a nickel–citrate complex, $K_2[Ni(C_6H_5O_7)(H_2O)_2]_2 \cdot 4H_2O$. Inorg. Chim. Acta 78, 281–285.

Bani, A., Echevarria, G., Sulce, S., Morel, J.-L., Mullai, A., 2007. In-situ phytoextraction of Ni by a native population of *Alyssum murale* on an ultramafic site (Albania). Plant Soil 79–89.

Boyd, R.S., Martens, S.N., 1992. The raison d'être for metal hyperaccumulation by plants. In: Baker, A.J.M., Proctor, J., Reeves, R.D. (Eds.), The Vegetation of Ultramafic (Serpentine) Soils. Intercept Ltd., Andover, GB, pp. 279–289.

Boyd, R.S., Martens, S.N., 1998. The significance of metal hyperaccumulation for biotic interactions. Chemoecology 8, 1–7.

Boyd, R.S., 2004. Ecology of metal hyperaccumulation. New Phytol. 162, 563–567.

Broadhurst, C.L., Chaney, R.L., Angle, J.S., Maugel, T.K., Erbe, E.F., Murphy, A.C., 2004. Simultaneous hyperaccumulation of nickel, manganese, and calcium in *Alyssum* leaf trichomes. Environ. Sci. Technol. 38, 5797–5802.

Callahan, D.L., Kolev, S.D., O'Hair, R.A.J., Salt, D.E., Baker, A.J.M., 2007. Relationships of nicotianamine and other amino acids with nickel, zinc and iron in *Thlaspi* hyperaccumulators. New Phytol. 176, 836–848.

Chaney, R.L., Malik, M., Li, Y.-M., Brown, S.L., Brewer, E.P., Angle, J.S., Baker, A.J.M., 1997. Phytoremediation of soil metals. Curr. Opin. Biotechnol. 8, 279–284.

Chardot, V., Massoura, S.T., Echevarria, G., Reeves, R.G., Morel, J.-L., 2005. Phytoextraction potential of the nickel hyperaccumulators *Leptoplax emarginata* and *Bornmuellera tymphea*. Int. J. Phytorem. 7, 323–336.

Chardot, V., Echevarria, G., Gury, M., Massoura, S.T., Morel, J.-L., 2007. Nickel bioavailability in an ultramafic toposequence in the Vosges Mountains (France). Plant Soil 293, 7–21.

Clemens, S., 2001. Molecular mechanisms of plant metal tolerance and homeostasis. Planta 212, 475–486.

Collins, R.N., 2004. Separation of low-molecular mass organic acid–metal complexes by high-performance liquid chromatography. J. Chromatogr. 1059, 1–12.

Colpas, G.J., Maroney, M.J., Bagyinka, C., Kumar, M., Willis, W.S., Suib, S.L., Baidya, N., Mascharak, P.K., 1991. X-ray spectroscopic studies of nickel complexes, with application to the structure of nickel sites in hydrogenases. Inorg. Chem. 30, 920–928.

Costa, C., Morel, J.-L., 1993. Cadmium uptake by *Lupinus albus* (L): cadmium excretion, a possible mechanism of cadmium tolerance. J. Plant Nutr. 16, 1921–1929.

Echevarria, G., Massoura, S.T., Steckerman, T., Becquer, T., Schwartz, C., Morel, J.-L., 2006. Assessment and control of the bioavailability of nickel in soils. Environ. Toxicol. Chem. 25, 643–651.

Gérard, E., Echevarria, G., Steckerman, T., Morel, J.-L., 2000. Cadmium availability to three plant species varying in cadmium accumulation pattern. J. Environ. Qual. 29, 1117–1123.

Hanson, B., Garifullina, G.F., Lindblom, S.T., Wangeline, A., Ackley, A., Krämer, K., Norton, A.P., Lawrence, C.B., Pilon-Smits, E.A.H., 2003. Selenium accumulation protects *Brassica juncea* from invertebrate herbivory and fungal infection. New Phytol. 159, 461–469.

Ingle, R.A., Mugford, S.T., Rees, J.D., Campbell, M.M., Smith, A.C., 2005. Constitutively high expression of the histidine biosynthetic pathway contributes to nickel tolerance in hyperaccumulator plants. Plant Cell 17, 2016–2089.

Jones, D.L., 1998. Organic acids in the rhizosphere – a critical review. Plant Soil 205, 25–44.

Kersten, W.J., Brooks, R.R., Reeves, R.G., Jaffré, T., 1980. Nature of nickel complexes in *Psychotria douarrei* and other nickel-accumulating plants. Phytochemistry 19, 1963–1965.

Koninsberger, D.C., Prins, R., 1988. X-ray Absorption. Principles, Applications, Techniques of EXAFS, SEXAFS and XANES. John Wiley & Sons Inc., New York, 673 p.

Krämer, U., Cotter-Howells, J.D., Charnock, J.M., Baker, A.J.M., Smith, J.A.C., 1996. Free histidine as a metal chelator in plants that accumulate nickel. Nature 379, 635–638.

Krämer, U., Grime, G.W., Smith, J.A.C., Hawes, C.R., Baker, A.J.M., 1997. Micro-PIXE as a technique for studying nickel localization in leaves of the hyperaccumulator plant *Alyssum lesbiacum*. Nucl. Instrum. Meth. Phys. Res., Sect. B 130, 346–350.

Krämer, U., Pickering, I.J., Prince, R.C., Raskin, I., Salt, D.E., 2000. Subcellular localization and speciation of nickel in hyperaccumulator and non-accumulator *Thlaspi* species. Plant Physiol. 122, 1343–1353.

Küpper, H., Zhao, F.J., McGrath, S.P., 1999. Cellular compartmentation of zinc in leaves of the hyperaccumulator *Thlaspi caerulescens*. Plant Physiol. 119, 305–331.

Küpper, H., Lombi, E., Zhao, F.J., McGrath, S.P., 2000. Cellular compartmentation of cadmium and zinc in relation to other elements in the hyperaccumulator *Arabidopsis halleri*. Talanta 212, 75–84.

Küpper, H., Lombi, E., Zhao, F.J., Wieshammer, G., McGrath, S.P., 2001. Cellular compartmentation of nickel in the hyperaccumulators *Alyssum lesbiacum*, *Alyssum bertolonii* and *Thlaspi goesingense*. J. Exp. Bot. 52, 2291–2300.

Lee, J., Reeves, R.G., Brooks, R.R., Jaffré, T., 1977. Isolation and identification of a citrato-complex of nickel from nickel-accumulating plants. Phytochemistry 16, 1503–1505.

Lee, J., Reeves, R.G., Brooks, R.R., Jaffré, T., 1978. The relation between nickel and citric acid in some nickel-accumulating plants. Phytochemistry 17, 1033–1035.

Mari, S., Gendre, D., Pianelli, K., Ouerdane, L., Lobinski, R., Briat, J.-F., Lebrun, M., Czernic, P., 2006. Root-to-shoot long distance circulation of nicotianamine and nicotinanamine–nickel chelates in the metal hyperaccumulator *Thlaspi caerulescens*. J. Exp. Bot. 57, 4111–4122.

Martell, A.E., Hancock, R.D., 1996. Metal Complexes in Aqueous Solutions. Plenum Press, New York, 264 p.

McNear Jr., D.H., Chaney, R.L., Sparks, D.L., 2007. The effects of soil type and chemical treatment on nickel speciation in refinery enriched soils: a multi-technique investigation. Geochim. Cosmochim. Acta 71, 2190–2208.

Mesjasz-Przybylowicz, J., Balkwill, K., Przybylowicz, W.J., Annegarn, H.J., 1994. Proton microprobe and X-ray microfluorescence investigations of nickel distribution in serpentine flora from South Africa. Nucl. Instrum. Meth. Phys. Res., Sect. B 89, 208–212.

Mesjasz-Przybylowicz, J., Przybylowicz, W.J., 2001. Phytophagous insects associated with the Ni-hyperaccumulating plant *Berkheya coddii* (Asteracea) in Mpumalanga, South Africa. S. Afr. J. Sci. 97, 596–598.

Mesjasz-Przybylowicz, J., Przybylowicz, W.J., Pineda, C.A., 2001. Nuclear microprobe studies of elemental distribution in apical leaves of the Ni hyperaccumulator *Berkheya coddii*. S. Afr. J. Sci., 97.

Newville, M., 2001. EXAFS analysis using FEFF and FEFFIT. J. Synchr. Rad. 8, 96–100.

Ouerdane, L., Mari, S., Czernic, P., Lebrun, M., Lobinski, R., 2006. Speciation of non-covalent nickel species in plant tissue extracts by electrospray Q-TOFMS/MS after their isolation by 2 D size exclusion-hydrophilic interaction LC (SEC-HILIC) monitored by ICP-MS. J. Anal. At. Spectrom. 21, 676–683.

Perronnet, K., Schwartz, C., Morel, J.-L., 2003. Distribution of cadmium and zinc in the hyperaccumulator *Thlaspi caerulescens* grown on multicontaminated soil. Plant Soil 249, 19–25.

Persans, M.W., Yan, X., Patnoe, J.-M.M.L., Krämer, U., Salt, D.E., 1999. Molecular dissection of the role of histidine in nickel accumulation in *Thlaspi goesingense* (Halacsy). Plant Physiol. 121, 1117–1126.

Pollard, A.J., Baker, A.J.M., 1997. Deterrence of herbivory by zinc hyperaccumulation in *Thlaspi caerulescens* (Brassicaceae). New Phytol. 135, 655–658.

Prasad, M.N.V., 2005. Nickelophilous plants and their significance in phytotechnologies. Braz. J. Plant. Physiol. 17, 113–128.

Psaras, G.K., Constantinidis, T., Cotsopoulos, B., Manetas, Y., 2000. Relative abundance of nickel in the leaf epidermis of eight hyperaccumulators: evidence that the metal is excluded from both guard cells and trichomes. Ann. Bot. 86, 73–78.

Ravel, B., Newville, M., 2005. ATHENA, ARTEMIS, HEPHAESTUS: data analysis for X-ray absorption spectroscopy using IFEFFIT. J. Synchr. Rad. 12, 537–541.

Robinson, B.H., Lombi, E., Zhao, F.J., McGrath, S.P., 2003. Uptake and distribution of nickel and other metals in the hyperaccumulator *Berkheya coddii*. New Phytol. 158, 279–285.

Sakurai, T., Iwasaki, H., Katano, T., Nakahashi, Y., 1978. Bis(*L*-histidinato)nickel(II) monohydrate. Acta Crystallogr. C: Cryst. Struct. Commun. B34, 660–662.

Salt, D.E., Prince, R.C., Baker, A.J.M., Raskin, I., Pickering, I.J., 1999. Zinc ligands in the metal hyperaccumulator *Thlaspi caerulescens* as determined using X-ray absorption spectroscopy. Environ. Sci. Technol. 33, 713–717.

Sarret, G., Vangronsveld, J., Manceau, A., Musso, M., D'Haen, J., Menthonnex, J.-J., Hazemann, J.-L., 2001. Accumulation forms of Zn

and Pb in *Phaseolus vulgaris* in the presence and absence of EDTA. Environ. Sci. Technol. 35, 2854–2859.

Sarret, G., Saumitou-Laprade, P., Bert, V., Proux, O., Hazemann, J.-L., Traverse, A., Marcus, M.A., Manceau, A., 2002. Forms of zinc accumulated in the hyperaccumulator *Arabidopsis halleri*. Plant Physiol. 130, 1825–1826.

Sarret, G., Schroeder, W.H., Marcus, M.A., Geoffroy, N., Manceau, A., 2003. Localization and speciation of Zn in mycorrhized roots by m-SXRF and m-EXAFS. J. Phys. IV (107), 1193–1196.

Schaumlöffel, D., Ouerdane, L., Bouyssiere, B., Lobinski, R., 2003. Speciation analysis of nickel in the latex of a hyperaccumulating tree *Sebertia accuminata* by HPLC and CZE with ICP MS and electrospray MS-MS detection. J. Anal. At. Spectrom. 18, 120–127.

Shallari, S., Schwartz, C., Hasko, A., Morel, J.-L., 1998. Heavy metals in soils and plants of serpentine and industrial sites of Albania. Sci. Total Environ. 209, 133–142.

Strathmann, T.J., Myneni, S.C.B., 2004. Speciation of aqueous Ni(II)-carboxylate and Ni(II)-fulvic acid solutions: combined ATR-FTIR and XAFS analysis. Geochim. Cosmochim. Acta 68, 3441–3458.

Ueno, D., Ma, J.F., Iwashita, T., Zhao, F.J., McGrath, S.P., 2005. Identification of the form of Cd in the leaves of a superior Cd-accumulating ecotype of *Thlaspi caerulescens* using ^{113}Cd-NMR. Planta 221, 928–936.

Vacchina, V., Mari, S., Czernic, P.L.M., Pianelli, K., Schaumlöffel, D., Lebrun, M., Lobinski, R., 2003. Speciation of nickel in a hyperaccumulating plant by high-performance liquid chromatography – inductively coupled plasma mass spectrometry and electrospray MS/MS assited by cloning using yeast complementation. Anal. Chem. 75, 2740–2745.

Webb, S.M., Gaillard, J.-F., Ma, L.Q., Tu, C., 2003. XAS speciation of arsenic in a hyper-accumulating fern. Environ. Sci. Technol 37, 754–760.

Zhou, Z.-H., Ye, J.-J., Deng, Y.-F., Wang, G., Gao, J.-X., Wan, H.-L., 2002. Monomeric and polymeric nickel complexes of malate: X-ray crystal structure of polymeric homochiral *S*-malato nickel (II), $[-Ni(S-Hmal)(H_2O)_2]_n \cdot nH_2O$. Polyhedron 21, 787–790.